Available online at www.CivileJournal.org

Civil Engineering Journal

(E-ISSN: 2476-3055; ISSN: 2676-6957)

Vol. 11, No. 08, August, 2025

Innovative Advancements in Construction: The Sustainable Promise of Aerated Concrete Incorporating Fly Ash and River Sand

Maroosha Larik [1*], Aneel Kumar [1], Tauha Hussain Ali [1], Rimsha Larik [2]

[1] Department of Civil Engineering, Mehran University of Engineering and Technology, Jamshoro, 76060, Pakistan.

[2] National Centre of Excellence in Analytical Chemistry, University of Sindh, Jamshoro, 76080, Pakistan.

Received 21 February 2025; Revised 13 June 2025; Accepted 19 June 2025; Published 01 August 2025

Abstract

Aerated Concrete, or lightweight concrete, is primarily used in construction work for non-load-bearing structures and is typically produced with cement as a primary binding material. Cement production accounts for 7 to 8% of the environmental CO_2 emissions. Furthermore, the dumping of industrial waste and the consumption of aggregates disrupt the environment and ecosystem. This research aims at developing sustainable AC by partially substituting cement with FA and hill sand with IRS while maintaining the fundamental properties of aerated concrete. The study was conducted to investigate the physical and chemical properties of the materials and the physical and mechanical properties of aerated concrete. Variations of fly ash, i.e., 10%-70%, were incorporated as a CRM to get optimum FA usage in terms of density and compressive strength. Optimum FA was incorporated as CRM and IRS as sand replacement, used in four variations, i.e., 10% - 25%. Specimens were cured using the conventional curing method and autoclaving for NAAC and AAC, considering both manufacturing processes, CO_2 emissions and time limitations in respective curing methods. Conventional curing was performed at 7, 14, and 28 days, while autoclaving was performed at various pressures, i.e., 0.5 bar, 1 bar, and 1.5 bar. The optimum compressive strength of AAC and NAAC was achieved when 20% of the IRS and 50% of FA were replaced with hill sand and cement, respectively, for both AAC and NAAC. Additionally, approximately 32% and 39.3% of CO_2 emissions were reduced with 50% FA and 20% river sand replacement with cement for AAC and NAAC specimens. Although AAC demonstrated slightly lower water absorption due to densification through autoclaving, NAAC performed satisfactorily in offering a more cost-effective and energy-efficient alternative.

Keywords: Autoclave Aerated Concrete; Non-Autoclaved Aerated Concrete; Aluminum Powder; Strength Characteristics; River Sand.

1. Introduction

The demand for energy-efficient buildings is increasing progressively due to growing environmental concerns and economic considerations. Heating and cooling systems account for a significant proportion of a building's operational costs over its lifecycle, especially in regions characterized by pronounced temperature fluctuations [1]. Consequently, the selection of appropriate insulating materials is critical for optimizing energy efficiency and minimizing thermal losses in building construction.

Aerated concrete (AC) is a specific type of lightweight concrete characterized by its reduced density. It generally consists of binders like cement and lime, silica-rich supplemental cementitious materials (e.g., slag, fly ash, or silica fume), fine aggregates (e.g., silica or quartz), an expansion agent (usually aluminum powder), and water [2-4]. In comparison to traditional construction materials, AC is cost-effective due to its lightweight properties that diminish

* Corresponding author: maroosha.larik@faculty.muet.edu.pk

http://dx.doi.org/10.28991/CEJ-2025-011-08-019

structural requirements, and it utilizes waste resources like fly ash, enhancing both economic efficiency and environmental sustainability. Aerated concrete's remarkable durability and intrinsic insulation properties enable it to meet the growing demands for comfort, energy efficiency, and sustainability, particularly in the context of reducing carbon emissions. The material composition and proportions of AC may differ based on its specific application, such as improving thermal insulation, reducing dead load, or enhancing energy efficiency. Owing to its lightweight characteristics, AC is widely employed in various building applications. Furthermore, when load-bearing capacity is not a critical factor, AC can be utilized for both external and internal applications [4]. In light of environmental concerns and the rising need for efficient construction materials, researchers and industry professionals are diligently investigating alternatives that improve performance, durability, and environmental sustainability [5-7].

A prominent feature of AC is its porous structure. The pores are formed via a chemical reaction between aluminum powder and alkalis in the cementitious mixture, resulting in the production of hydrogen gas and the formation of a lightweight foamed matrix [8]. This chemical reaction generates millions of well-distributed, consistently sized air gaps that become trapped inside the concrete mixture, yielding a porosity range of 75% to 90% for AC [9]. This distinctive material composition allows AC to demonstrate remarkable characteristics, such as a low thermal conductivity (λ) of 0.15 to 0.20 W/m·K, an oven-dry density of 240 to 1900 kg/m³, and a compressive strength generally between 2.5 and 10 MPa [10-12]. The reduction of energy usage and heating expenses has been a central concern for several decades. The implementation of air conditioning in construction and renovation projects decreases building energy consumption, as its intrinsic insulating capabilities negate the necessity for supplementary insulation [5, 13, 14].

In the future, increased attention will be directed into evaluating the carbon footprint of a building during its whole existence [15]. The quantity of binder (such as cement or quicklime) used during the utilization phase directly correlates with the significant reduction in AC's carbon footprint or global warming potential (GWP) via carbonization [16]. AC is classified as either Non-Autoclaved Aerated Concrete (NAAC) or Autoclaved Aerated Concrete (AAC) based on the curing method employed. Conventional curing (moist curing) is utilized for NAAC, whereas autoclaving is applied for AAC. The curing process and its duration directly affect key properties of aerated concrete, such as compressive strength, drying shrinkage, and absorption characteristics. AAC demonstrates diminished density, minimized shrinkage, enhanced fire resistance, and lower thermal conductivity relative to non-autoclaved alternatives [17-19]. AAC is acknowledged for its capacity to fulfil rigorous standards for energy efficiency, occupant comfort, and sustainability. Its durability and thermal insulation properties substantially diminish carbon emissions, making it a preferred material for sustainable construction [20]. Conversely, the NAAC provides benefits by simplifying production and minimizing expenses. NAAC is produced using traditional curing techniques, leading to reduced energy usage relative to AAC, while maintaining product safety [21]. The strength increase in conventionally cured specimens is comparatively delayed because to the presence of unstable calcium silicate hydrate (CSH) phases. NAAC is generally cured at ambient temperatures, which impedes reaction kinetics and results in the development of less stable phases. With time, exposure to atmospheric elements like moisture and carbonation facilitates the recrystallization of the initially needle-like microstructure into more stable hexagonal or plate-like phases, ultimately evolving into a denser, blocky crystalline structure as the material seeks thermodynamic stability. Conversely, AAC, exposed to elevated temperatures (about 180°C) and high-pressure environments (10–12 bar), enables hydrothermal interactions between lime and silica- or alumina-rich materials, hence fostering the development of the stable CSH phase. This phase maintains stability throughout time, offering AAC enhanced compressive strength and less drying shrinkage relative to NAAC. Researchers have thoroughly investigated the hydrothermal processes happening during autoclaving to enhance material performance [22, 23].

AAC has demonstrated exceptional capability in fulfilling rigorous requirements for energy efficiency, occupant comfort, and sustainability. Its exceptional durability and intrinsic thermal insulation capabilities significantly contribute to the reduction of carbon emissions, making it a preferred material for sustainable construction [20]. Researchers have recorded substantial variations in suggested autoclaving parameters, with pressures varying from 4 to 16 MPa and curing times spanning 8 to 16 hours [23-25]. By simplifying the production process and reducing product prices, NAAC offers a significant advantage over traditional AAC. The conventional curing process is utilized in the production of NAAC. Consequently, NAAC distinguishes itself from AAC by ensuring product safety and reduced energy use in comparison to AAC.

Mechanical properties are crucial for the structural application of aerated concrete, with compressive strength being a key parameter influenced by various factors, including mix design, material quality and type, curing conditions and duration, and the type of aerating agent used. These factors affect the porosity of aerated concrete, which in turn governs its compressive strength. As a result, the density of AC is directly correlated with its compressive strength. It is attributed to the formation of a large number of micro-pores, reported by Narayan and Ramamurthy [21] reported that AAC with a density of 700 kg/m³ exhibited compressive strength in the range of 3.9–8.5 MPa, whereas at a reduced density of 400 kg/m³, compressive strength declined to 1.3–2.8 MPa. The integration of sustainable materials in AC production has garnered significant attention for its potential to mitigate environmental impact. Lashari et al. [26] Investigated the partial replacement of cement with FA in AAC, demonstrating its effectiveness in reducing carbon emissions without

compromising compressive strength. Ramamurthy & Narayan [27] reported that an increase in the lime-cement ratio and fly ash content leads to higher drying shrinkage in both AAC and NAAC. However, autoclaving significantly reduces drying shrinkage by approximately six times. It was also observed that the drying shrinkage of AAC and NAAC containing fly ash is about 5 to 7 times greater than that of mixes using sand as the sole filler—several studies [17-19, 28] have reported a relationship between thermal conductivity and density in concrete, reported that the thermal conductivity of AAC ranges from 0.08 to 0.11 W/m·K at 25°C, with corresponding density values between 270 and 500 kg/m³. Albayrak et al. [29] also examined the role of the autoclaving process in ensuring a consistent pore morphology, which is essential for preserving these thermal properties. Jerman et al. [30] further confirmed that the thermal conductivity of AAC is influenced by both density and moisture content, with higher conductivity observed in denser and more saturated specimens. Durability under extreme environmental conditions also remains a key focus in aerated concrete—freeze-thaw resistance studies by Jerman et al. [30] demonstrated that moisture content plays a significant role in performance. Dry AAC samples exhibited minimal strength loss after 50 freeze-thaw cycles, whereas fully saturated samples experienced severe deterioration, particularly in lower-density specimens. These findings are consistent with those of Tikalsky et al. [31], who reported that AAC with a moisture content below 16%, a density between 500–600 kg/m³, and compressive strength of 1–2 MPa exhibited favorable freeze-thaw resistance.

Several studies have explored the use of various waste products in AAC to replace cement and sand [32-34]. Dey et al. [35] examined recent advancements in autoclaved aerated concrete (AAC), emphasizing its viability as a sustainable substitute for conventional building materials. The study indicates that AAC possesses excellent thermal insulation, minimal carbon emissions, and adequate strength for construction purposes. The authors examined the utilization of waste materials such as rice husk ash, bottom ash, and zeolite in AAC to mitigate environmental effects and conserve natural resources. They revealed that using components such as fibers, nano-graphene, and phase change materials (PCMs) can enhance the structural integrity and thermal comfort of structures constructed with AAC. In a related work, Wei et al. [36] investigated the application of titanium gypsum (TG) as a partial replacement for fly ash in autoclaved aerated concrete (AAC). Despite increased TG levels resulting in reduced strength, the study revealed that performance may be reinstated through wet grinding and the use of additives such as slag and silica fume. Their findings demonstrated that TG may chemically bond during autoclaving to produce stable sulfur-rich tobermorite, highlighting its potential as an environmentally sustainable material in AAC. Sun et al. [37] investigated the advancement of carbonated aerated concrete (CAC) utilizing steel slag as a primary binder to reduce energy consumption and carbon emissions. Their investigation focused on the impact of various curing regimens and binder ratios on strength development and carbonation. The research indicated that curing in moderate humidity, succeeded by CO_2 exposure, achieves an optimal equilibrium between pre-hydration and carbonation, hence improving strength and durability. The optimized CAC demonstrated favorable outcomes for compressive strength, air-void distribution, and environmental impact, positioning it as a viable option for sustainable building.

Xie et al. [29] examined the replacement of fly ash in autoclaved aerated concrete (AAC) with granite stone powder (GSP) and steel slag (SS) to enhance sustainability. The researchers concentrated on optimizing the calcium-to-silicon (Ca/Si) ratio, which significantly influences the formation of tobermorite, an essential mineral contributing to the strength of AAC. The results indicated that increasing the Ca/Si ratio from 0.63 to 0.92 enhanced compressive strength by 48.6% (reaching 5.2 MPa) and decreased bulk density. The research indicated that increased Ca/Si ratios resulted in the conversion of tobermorite from a needle-like to a denser, network-like crystalline structure, hence improving the mechanical characteristics of AAC. This method substantially reduced carbon emissions and energy consumption, hence validating the environmental advantages of employing GSP and SS in AAC manufacture. Chen et al. [38] formulated a sustainable non-autoclaved aerated concrete (NAAC) utilizing rockwool furnace bottom slag (RWFBS) as a binder. The research demonstrated the impact of water-to-solid ratio, calcium stearate (as a foam stabilizer), and aluminum powder on compressive strength and pore structure. The maximum strength (2.91 MPa) and ideal pore structure were attained at a 1.4 stabilizer-to-aluminum ratio. CT imaging demonstrated a shift from isolated to interconnected pores as aluminum content increased, resulting in increased water absorption and reduced strength. This study illustrates the efficient utilization of industrial waste in geopolymer-based NAAC, exhibiting favourable mechanical and environmental properties. However, the production of AAC requires significant energy input and specialized autoclaving equipment, which increases both costs and environmental impact. In contrast, NAAC offers similar benefits while potentially reducing energy consumption and equipment costs [39, 40].

Further, researchers have investigated river sand (RS) as a sustainable alternative to hill sand in conventional concrete for mitigating the depletion of natural resources [41]. However, its use in conventional concrete reduces strength and durability, limiting its application in high-strength structures [42, 43]. AC, characterized by lower strength requirements, offers a promising avenue for river sand utilization, yet this potential remains largely unexplored. While extensive research has focused on incorporating materials such as recycled aerated concrete, fly ash, rice husk, and bagasse ash as partial or complete substitutes for hill sand in AC [16, 44, 45], the use of river sand in AC has received limited attention. This knowledge gap highlights the need for further investigation into the viability of river sand in AC production, which could contribute to more sustainable construction practice.

Despite this, research on NAAC remains limited, and there is a lack of comparative studies between AAC and NAAC, particularly in terms of their properties when using river sand as a partial replacement for natural hill sand. This paper aims at filling this gap by examining NAAC's economic and environmental advantages over AAC and investigating the differences in their properties when river sand is utilized.

The structure of this paper is organized as follows: Section 2 outlines the research methodology, including material characterization and experimental procedures. Section 3 presents the results, including dry density and compressive strength, comparative analysis of AAC and NAAC, including compressive strength comparison and an environmental impact assessment. Finally, Section 4 summarizes the key conclusions of the study.

2. Research Methodology

2.1. Physical and Chemical Composition of Materials

This experimental study used locally available hill sand obtained from the Bholari plant in Jamshoro District, Pakistan. Hill sand was passed through a 850-micron sieve and retained on a 600-micron sieve for usage. River sand was sourced from downstream of the Kotri barrage, the last barrier on the Indus River before it merges with the Arabian Sea, locally known as Indus River Sand (IRS), Figure 1 illustrates the particle size distribution (PSD) curves of two types of sands, i.e. Hill Sand and Indus River Sand (IRS), evaluated with a laser particle analyzer. The PSD curves are represented with particle size (D, in mm) on the logarithmic scale (x-axis) and percentage finer (%) on the y-axis. This graph illustrates the gradation and fineness properties of the sands, which are crucial to the effectiveness of mortar mixtures. The blue curve denotes the PSD of Hill Sand, whereas the red curve signifies Indus River Sand (IRS). The D-values (D_{10}, D_{30}, D_{60}), essential indications of particle size distribution, are indicated on each curve. These numbers denote the particle diameters at which 10%, 30%, and 60% of the sample (by weight) pass the sieve, respectively.

The particle size distribution curve of hill sand reveals D_{10}, D_{30}, and D_{60} values of 0.63 mm, 0.74 mm, and 1.11 mm, respectively. The PSD curve of Hill Sand exhibits a steep slope, signifying a limited range of particle sizes. The In dus River Sand curve is consistently graded, exhibiting D_{10}, D_{30}, and D_{60} values of 0.08 mm, 0.169 mm, and 0.24 mm, respectively. The sand from the Indus River is finer than that from the hills. Hill Sand has poor grading, characterized by a steeper curve and closely aligned D-values, indicating minimal variance in particle sizes. On the other hand, IRS is uniformly graded graded, which may compromise stability in construction applications if utilized excessively. Physical properties of the Indus River sand and the hill sand are provided in Table 1. While the chemical composition is presented in Table 2. The energy dispersive spectroscopy (EDS) of Indus River Sand (IRS) is shown in Figure 2. EDS can detect elements in a material. The chemical composition of IRS aligns with that of river sands from the Neelum River, Ravi River, Jhelum River, and Amazon River, as reported in the literature [46-48]. Table 1 also presents the physical properties of hill sand.

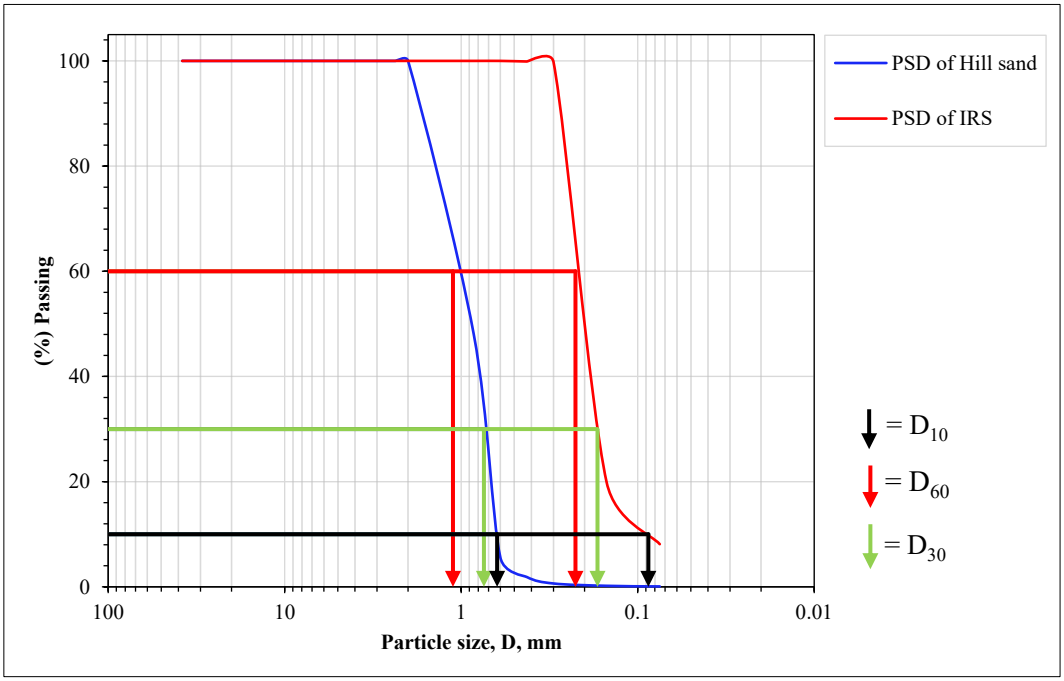

Figure 1. Particle Size Distribution (PSD) Curves for Hill Sand and River Sand

Table 1. Overview of Physical Properties of Materials

Property	Hill sand	IRS	Fly ash
Specific gravity	2.67	2.76	2.06
Fineness modulus	2.73	2.06	2.02
Water absorption	5.47%	8.3%	---
Color	Yellowish Orange	Silver Grey	Light Grey
Coefficient of Uniformity (Cu) × $Cu=D_{60}/D_{10}$	1.76	3	---
Coefficient of Curvature (Cc) × $Cc= D_{30}^2/D_{10} \times D_{60}$	0.783	1.48	---

Table 2. Oxide-Based Chemical Composition of Materials

Chemical	Fly ash%	OPC%	IRS%	Hill Sand	River Sands i.e. Amazon, Nile, Ravi, Jhelum [46-49]
SiO_2	51.64	16.26	76.12	55.57	52-81.03
Al_2O_3	22.65	3.174	6.94	9.56	7.48-20
Fe_2O_3	4.12	5.514	2.88	7.87	1.844-7.7
CaO	13.84	71.359	2.56	14.71	0.79-1.217
MnO	0.01	-	0.2	-	0.0318-0.08
K_2O	1.68	3.469	0.21	1.67	1.44-3.2
P_2O_5	0.62	-	2.54	-	0-0.21
MgO	-	1.343	-	-	0-1.8
Na_2O	-	-	-	-	0-0.78

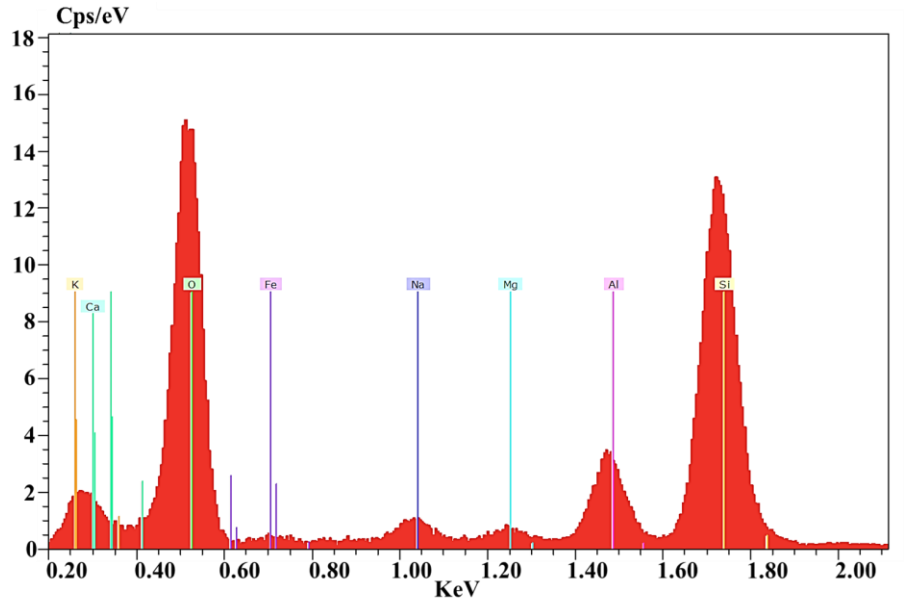

Figure 2. EDS Spectrum of Indus River Sand (IRS)

Ordinary Portland Cement (OPC) was used in this study. The chemical composition of the OPC is provided in Table 2, which conforms to ASTM C150 [50]. The cement bags were carefully stored in airtight containers to protect them from weathering effects. Fly ash (FA), a byproduct of coal combustion in thermal power plants, was used as a cement replacement material to enhance the eco-friendliness of the aerated concrete [51]. Particle size distribution curve of FA is shown in Figure 3. It exhibits pozzolanic properties, lightweight, and generates minimal heat during hydration [52]. Furthermore, it does not release carbon during alkaline reactions, making it a sustainable and environmentally friendly material [51, 52]. The EDS of FA and OPC is shown in Figures 4 and 5 respectively. The chemical composition of FA and OPC is shown in Table 2. According to ASTM C618-17 [53], it was concluded that FA was class F-type as sum of $SiO_2+Al_2O_3+Fe_2O_3>50\%$ and calcium oxide (CaO)<18%.

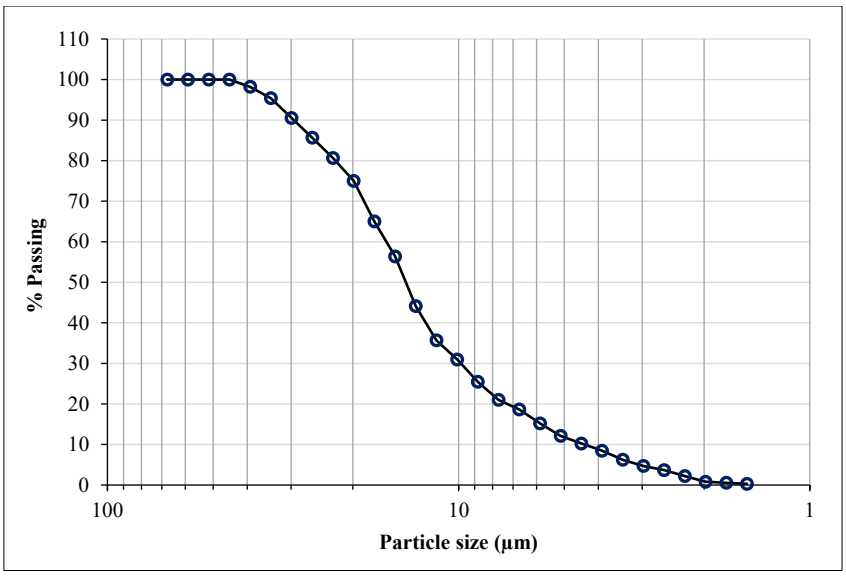

Figure 3. Particle Size Distribution (PSD) Curve of Fly Ash (FA)

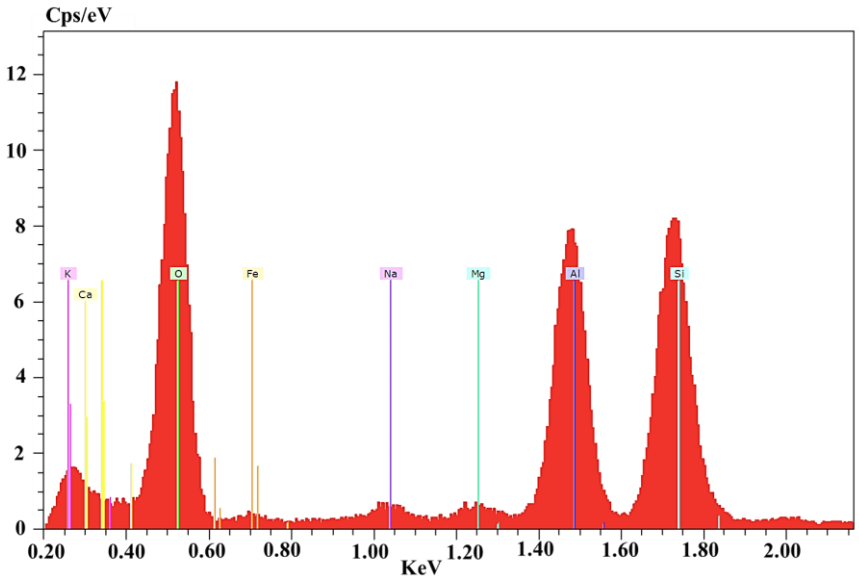

Figure 4. Energy Dispersive X-ray Spectroscopy (EDS) Spectrum of Fly Ash (FA)

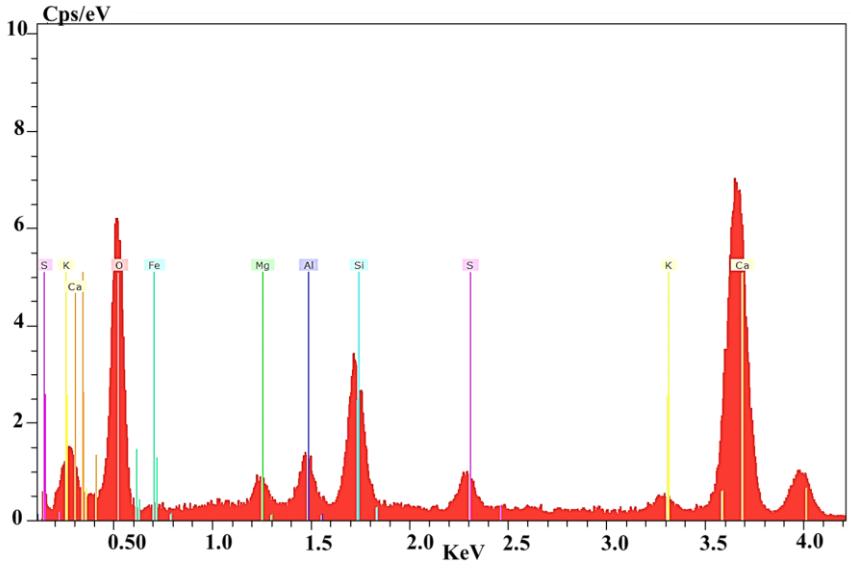

Figure 5. EDS Spectrum of Ordinary Portland Cement (OPC)

Aluminum powder (0.15 mm particle size), sourced from Karachi, was used as an aerating agent in both AAC and NAAC. In the absence of a standardized mix design code for aerated concrete, material quantities were determined through trial and error to optimize dry density and compressive strength. Aluminum content was tested at 0.3%, 0.4%, 0.5%, and 0.6% by weight of cement. At 0.3%, aeration was insufficient for mold expansion, while 0.5% and 0.6% caused excessive aeration and structural damage during de-molding. It was visually observed that the optimal aluminum content of 0.4% facilitated uniform expansion (20–40 mm), ensuring uniform void distribution, successful casting, and de-molding, and was adopted for the study.

Lime, sourced locally from the market, plays a critical role in the chemical reaction and overall performance of the material. Lime reacts with aluminum powder in the mixture to produce hydrogen gas bubbles. These bubbles cause the concrete to expand, creating a lightweight structure with air voids throughout, resulting in aerated concrete.

($2Al+3Ca(OH)_2+6H_2O \rightarrow 3CaO.\ Al_2O_3+3H_2$): This reaction helps form the cellular (air-filled) structure, giving the material its lightweight and insulating properties. Lime improves workability and helps in binding the particles together. Along with cement, it contributes to the setting and hardening of the aerated concrete. Lime maintains the alkalinity of the mixture, which is essential for proper chemical reactions and for enhancing the durability of the material.

2.2. Phase Structure and Crystallinity Confirmation

X-ray Diffraction (XRD) is a powerful technique for determining crystalline structure, phase composition, lattice parameters, and crystalline grain size. In this study, the crystalline nature of FA was confirmed by using X-ray Diffractometry with an MMA (GBC Scientific Equipment, Australia) model. The XRD analysis, shown in Figure 6, reveals that FA is primarily composed of inorganic materials, with quartz (SiO_2) and mullite ($3Al_2O_3 \cdot 2SiO_2$ or $Al_6Si_2O_{13}$) being the dominant crystalline phases along with minor hematite (Fe_2O_3) and a significant amount of amorphous silica (SiO_2). The XRD patterns show broad peaks, indicating of the amorphous nature of the majority of oxides in FA that contribute to its pozzolanic activity. When mixed with cement and water, FA produces concrete with a denser microstructure, exhibiting lower permeability compared to concrete made solely with cement. The XRD analysis also reveals sharp and intense peaks at 2θ values of approximately 15º, 20º, 45º, and 50º, 50º corresponding to the crystalline reflections of silica. These minor sharp peaks suggest that, upon exposure to high temperatures corresponding to the crystalline reflections of silica, FA undergoes a transition from an amorphous to a crystalline state, which results in a reduction in its pozzolanic reactivity, consistent with findings of previous studies [53]. This reduction in reactivity is attributed to the fact that crystalline phases generally exhibit lower surface reactivity.

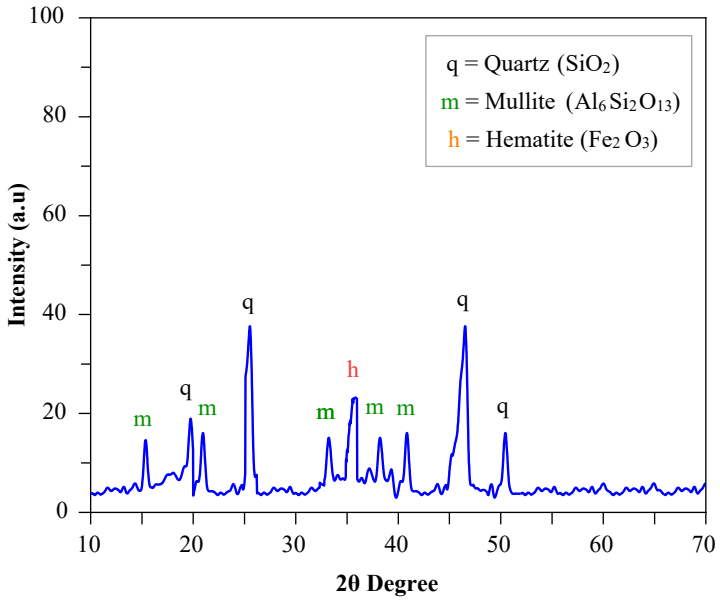

Figure 6. X-ray Diffraction (XRD) Analysis of Fly Ash (FA)

2.3. Surface Analysis

The advanced Scanning Electron Microscope (SEM) analysis provides critical visual insights into the surface morphology and microstructural characteristics of Fly Ash (FA), Indus River Sand (IRS), and Ordinary Portland Cement (OPC) as shown in Figures 7 to 9 respectively. These observations are fundamental to understanding their behavior and interaction in cementitious systems. SEM micrographs of FA are presented in Figure 7 at various magnifications to illustrate its particle characteristics. Figure 7-A provides a general overview, revealing a wide

particle size distribution. Many particles are generally spherical, a common morphological feature of FA. Figure 7-B offers a closer view, where the presence of both solid spherical particles and larger, hollow cenospheres is evident. Some smaller, irregularly shaped particles, potentially unburnt carbon, are also visible, adhering to or interspersed with the spherical particles.

The overall particle diameters range from a few microns to over 50 µm. This fine-grained nature, coupled with the predominantly spherical shape, contributes to a high surface area, suggesting FA is highly reactive in the hydration process, as also supported by its amorphous crystallographic structure (previously discussed with XRD results in Figure 6). Figure 7-C and Figure 7-D provide higher magnification details of the FA particle surfaces. These images show that while many particles are smooth and spherical, others exhibit a more complex, sometimes agglomerated or textured surface. This morphology facilitates good particle packing and contributes to the pozzolanic reactivity of FA. The elemental composition from EDS analysis Table 2, indicated that silicon (Si), aluminum (Al), calcium (Ca), and oxygen (O) are the predominant elements in the FA samples, forming various compounds. The presence of minor intensities of manganese (Mn), potassium (K), phosphorus (P), and iron (Fe) was also noted. The amorphous nature combined with this elemental composition and observed fine, spherical morphology underpins the reactivity of FA.

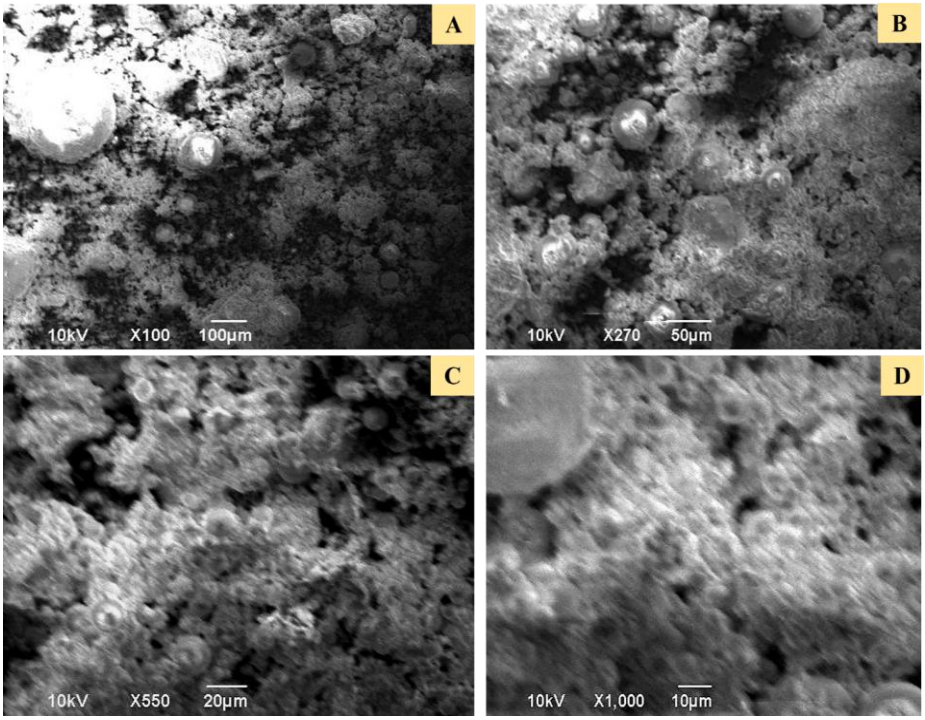

Figure 7. SEM images showcasing the morphology of Fly Ash FA at low and high resolution

The SEM images of IRS are presented in Figure 8 highlighting the distinct morphological characteristics of the sand particles. Figure 8-A shows a collection of IRS particles, revealing their predominantly angular to sub-angular shapes of almost uniform particle size. This angularity is indicative of mechanical weathering processes and a moderate degree of transport and abrasion in the riverine environment. Figures 8-B and 8-D provide clearer views of individual and grouped sand grains. The particles exhibit relatively defined edges and somewhat smooth, yet textured, surfaces. These images confirm the angular to sub-angular nature rather than spherical shapes. Figure 8-C offers a high-resolution view of a particle surface, detailing its texture, which includes minor irregularities and some pitting. The observed angular shapes can influence the interlocking behavior of particles within a concrete matrix. As indicated by EDS analysis (Table 2), over 75-80% of the IRS composition consists of silica (SiO_2), alumina (Al_2O_3), and oxygen (O_2), which is consistent with typical mineral compositions of river sands globally. Minor elements like manganese, potassium, calcium, phosphorus, and iron were also detected. The morphology observed in Figures 8-A and 8-D, specifically the angularity and size distribution, plays a role in the mechanical properties of aerated concrete. While angular particles can improve mechanical interlock, the overall particle size distribution and proportioning are critical; an optimal mix contributes to strength and density, whereas an imbalance or excessive fines/coarseness could lead to a deterioration in strength. The relatively smooth surfaces of these angular particles might influence the bond strength at the interfacial transition zone with the cement paste.

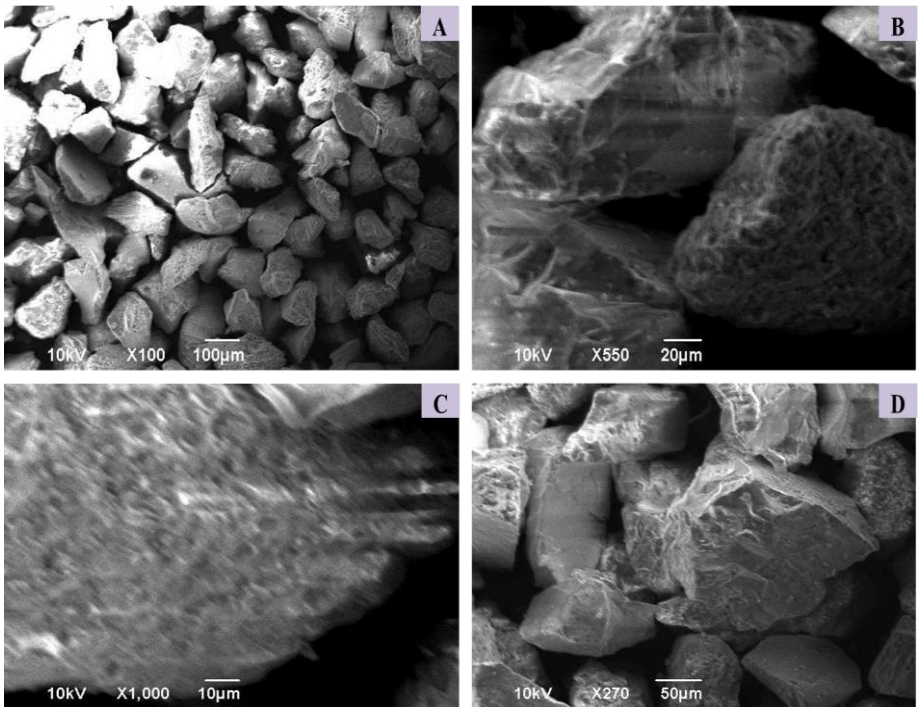

Figure 8. SEM images showcasing the morphology of Indus River Sand (IRS) at low and high resolution

SEM images of OPC are shown in Figure 9, illustrating its characteristic fine particulate nature. Figure 9-A and Figure 9-B reveal that OPC consists of significantly finer particles compared to both FA and IRS. These fine particles exhibit a strong tendency to form agglomerates, creating a "tufted" or clustered appearance. Figure 9-C and Figure 9-D at higher magnifications emphasize the extremely fine nature of the individual cement particles within these agglomerates. The overall structure appears porous due to the inter-particle spaces within the clumps. Individual OPC particles are typically angular and irregular, though their very small size (typically a few microns to tens of microns, but appearing much finer here due to fracture during sample prep or the inherent nature of the cement grains) results in a very high surface area. This high surface area, combined with their chemical composition, is crucial for the rapid hydration reactions that are characteristic of OPC. leading to setting and strength development in concrete. The agglomerated and somewhat porous structure seen in the micrographs provides numerous sites for water interaction, facilitating these hydration processes. The observed morphology is typical for unhydrated cement and contrasts sharply with the larger, more distinct particles of FA and IRS, highlighting its primary role as the main binder in concrete.

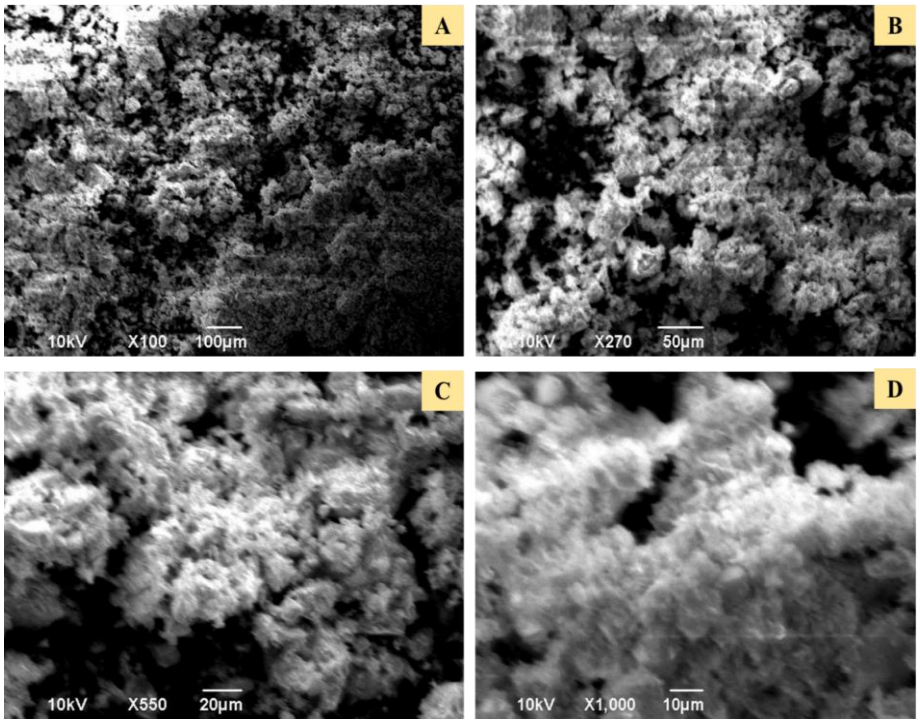

Figure 9. SEM images showcasing the morphology of OPC at low and high resolution

2.4. Experimental Work

In the first stage, the experimental work was performed through trial-and-error approach in a non-engineered manner for calculating the mix proportions of reference aerated concrete (Figure 10). A constant water to binder ratio of 0.55 was adopted after trials for proper aeration. Experimental work was conducted to incorporate FA as a cement replacement material (CRM) in accordance with ASTM C1693-11. Cement was partially replaced with FA in eight variations (0-70%), targeting AAC-4 grade which is ideal for internal partitions and external infill walls in framed structures, providing thermal insulation and fire resistance. The objective was to balance compressive strength and density reduction, as excessive FA could compromise structural integrity as quoted by Ramamurthy and Narayanan [27]. Trials replacing 0–70% of Ordinary Portland Cement (OPC) with FA (Figure 11) highlighted the importance of determining optimal replacement levels to maintain strength and functionality. At lower replacements, while compressive strength improved, density remained excessively high, which was unsuitable for lightweight concrete applications. Conversely, at higher replacements, density reduced, but the compressive strength fell below acceptable thresholds, rendering the material structurally inadequate. At 50% FA replacement, a balance was achieved, where the compressive strength (sufficient for structural applications) was retained while reducing density to a desirable level.

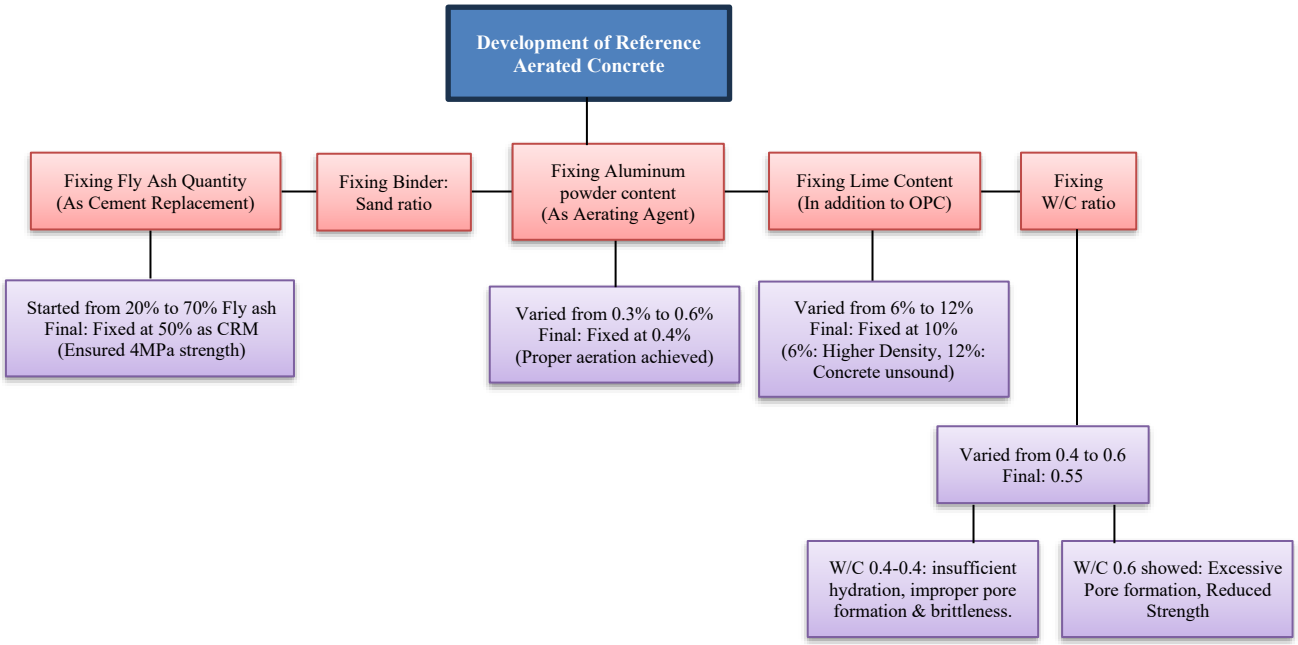

Figure 10. Experimental Procedure for Development of Reference Aerated Concrete (RF) Preparation

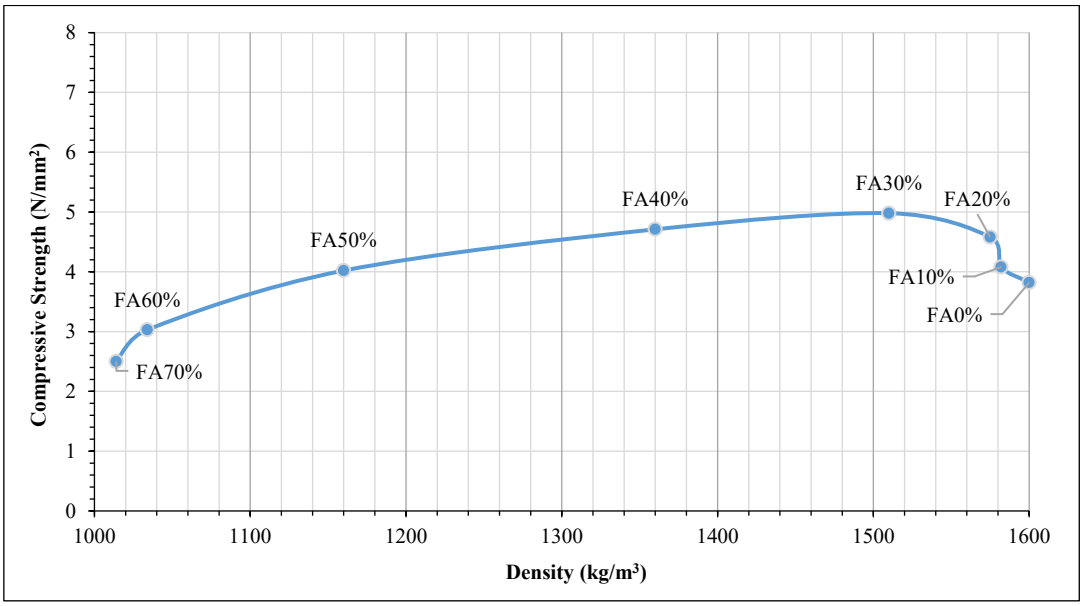

Figure 11. Compressive Strength vs. Density of Fly Ash (FA) as a Cement Replacement Material (CRM) with Varying Proportions. Notations: FA0%= 0%, FA10%= 10%, FA20%= 20%, FA30%= 30%, FA40%= 40%, FA50%= 50%, FA60%= 60%, FA70%= 70%.

Lime promotes the formation and stabilization of tiny air bubbles or pores in the concrete mixture, contributing to the lightweight and insulating properties of AC hence trials were done to determine the optimal lime content for aerated concrete. In this study, 10% lime by weight of OPC was incorporated in addition to OPC and FA. The binder-to-sand ratio was carefully optimized to achieve a balance between minimizing the weight of the concrete and ensuring adequate compressive strength. During the experimental process, it was observed that varying the sand content had significant effects on both the density and compressive strength of the aerated concrete. When the sand content was increased, the resulting concrete exhibited higher density due to the relatively higher specific gravity of sand compared to the binder. Although this led to improved compressive strength initially, the primary objective of producing lightweight AC was compromised. Excessive sand also hindered the formation of uniform air voids, thereby increasing weight of specimen. Hence, the mix design utilized a binder-to-sand ratio of 1:1.3. Additionally, 0.4% aluminum powder by weight of the binder, was added to create aeration. The mixing process was conducted using a laboratory-grade mortar mixer. First, the materials were dry mixed for 1 minute. Then water was added gradually to achieve a consistent base mortar, and the slurry was mixed for 30 seconds. During the mixing and forming stages, no significant issues such as segregation or abnormal setting time were observed, even with the finer particle size of IRS and FA. However, a slight reduction in flowability was noted with increasing IRS or FA content, which can be attributed to their higher surface area and increased water demand and Binder: Sand ratio was kept constant throughout. These variations were manageable and did not affect the workability of the mix significantly as Water: Binder ratio was kept higher. The slurry was poured into steel molds to set and demolded after 24 hours shown in (Figure 12).

Figure 12. Experimental Procedure for Compressive Strength Testing. (A-C) Mixing of materials: Preparation of the components for specimen formation. (D) Casting of cubes: Molding the prepared mixture into standardized shapes using steel molds. (E-F) Aeration of cubes: Ensuring uniform air distribution within the cubes. (G) Cutting of cubes: Shaping the specimens to meet uniformity standards for testing. (H) Steam curing: Application of controlled steam at specified pressures (0.5, 1, and 1.5 bar) for 8 hours, and by conventional curing for 7, 14, and 28 days. (I-J) Oven drying and compressive strength testing: Samples dried at 105 ± 5°C for 24 hours as per ASTM C642. (K) Final specimen preparation: Overview of the post-curing specimen, ready for final testing and analysis.

In the second stage, natural hill sand was partially replaced with IRS at replacement levels of 10%, 15%, 20%, and 25% to produce AAC and NAAC. These mix proportions are summarized in Table 3.

Table 3. Proportion of materials used in AAC and NAAC

Mix ID:	Binder: Sand	Water: Binder	Al (%) by wt: of binder	Cement (kg/m³)	Lime (kg/m³)	Fly Ash (kg/m³)	Sand (kg/m³)	IRS (kg/m³)	No. of Samples
RF	1:1.3	0.55	0.4	345	34.5	345	950	0	18
IRS5	1:1.3	0.55	0.4	345	34.5	345	902.5	47.5	18
IRS10	1:1.3	0.55	0.4	345	34.5	345	855	95	18
IRS15	1:1.3	0.55	0.4	345	34.5	345	807.5	142.5	18
IRS20	1:1.3	0.55	0.4	345	34.5	345	760	190	18
IRS25	1:1.3	0.55	0.4	345	34.5	345	712.5	237.5	18

In all, 90 cubes measuring 100 × 100 × 100 mm were employed in the investigation. For both AAC and NAAC, 18 cubes were cast as reference (RF) among them. In a similar manner, 72 cubes of IRS (10%–25%) were cast for AAC and NAAC after autoclaving for 8 hours at pressures of 0.5 bar, 1 bar, and 1.5 bar, and after 7, 14, and 28 days of regular curing, respectively. To assess the effects of various curing techniques, such as autoclaving versus traditional curing, a thorough comparison between NAAC and AAC was conducted in terms of density and compressive strength.

3. Results

3.1. Dry Density

In general, the finer IRS may also hinder proper aeration by reducing the escape paths for gas bubbles during the reaction with the aerating agent (e.g., aluminum powder), leading to a less porous structure.

As a result, the density of AC increases when IRS partially replaces Hill sand. Comparing the results of NAAC and AAC, NAAC has a higher density than AAC, but there is no more significant difference between both. Maximum density has been observed at 25% IRS replacement, which is 1193.5kg/m³ and 1185.3kg/m³ at 28 days of conventional curing and 1.5Bar autoclaving pressure, respectively, for NAAC and AAC, as shown in Figure 13. Compared to RF, NAAC has 2.9% higher density, and AAC has 3.4% higher density at 1.5 Bar pressure. This increment in density is because IRS is smaller in size and hence fills up the most pores in aerated concrete; the matrix's gradation level increases, which decreases aeration and increases the weight of the specimen.

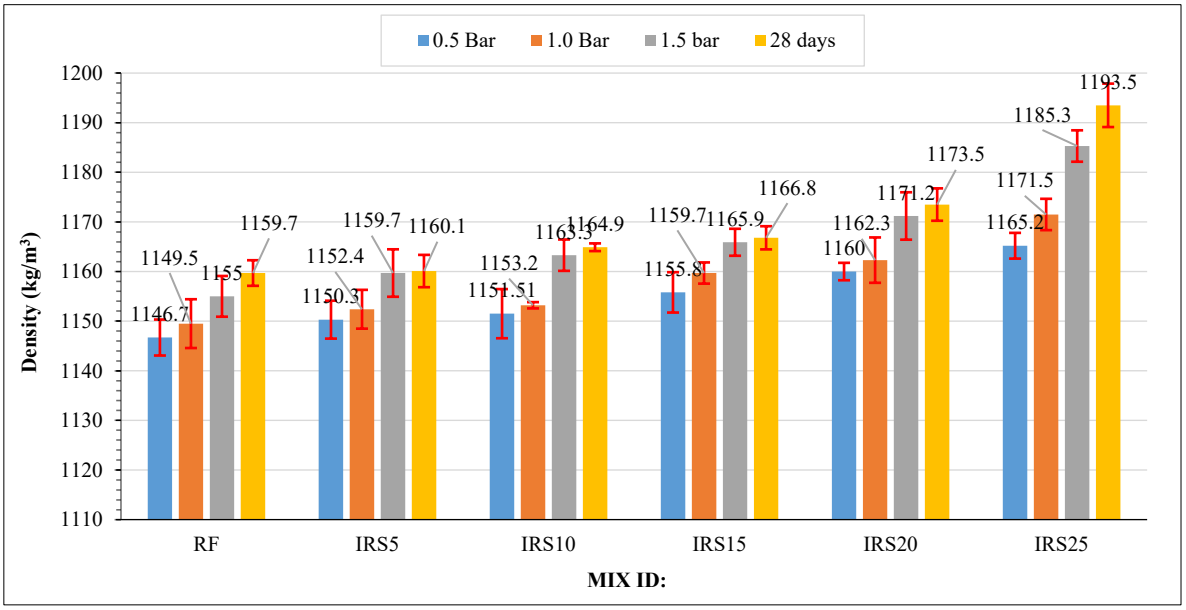

Figure 13. Dry Density Comparison of AAC and NAAC

3.2. Compressive Strength

The compressive strengths of NAAC and AAC are shown in Figures 14 and 15, respectively. The results indicate that compressive strength increases with the proportion of IRS up to 20% replacement of hill sand, beyond which further replacement led to a decline in strength. For NAAC, compressive strength of reference specimen was recorded 4.58MPa

and the highest compressive strength 5.9MPa was recorded at 20% IRS replacement at 28 days, showing increase of about 29% compressive strength, interpreted from Figure 14. For AAC, compressive strength was tested under autoclaving pressures of 0.5 bar, 1.0 bar, and 1.5 bar. The maximum compressive strength was achieved at 20% IRS replacement, recorded to be 6.28 MPa at 1.5bar autoclaving pressure with an increase of about 56% compared to reference specimen at 1.5bar autoclaving pressure, interpreted from Figure 15, compared to the reference specimen (RF) at 1.5 bar pressures, respectively. The increase in compressive strength may be attributed to the reduction in air voids within the aerated concrete. The finer particle size of Indus River sand, compared to hill sand, likely fills some of these voids (pores), leading to higher density and improved strength. This is also due to the reason that aeration reduces. Further, it is hypothesized that replacing more than 20% of hill sand with IRS may negatively impact concrete strength, as the smoother texture and uniform grading of IRS particles could reduce interlocking, thereby decreasing overall structural integrity.

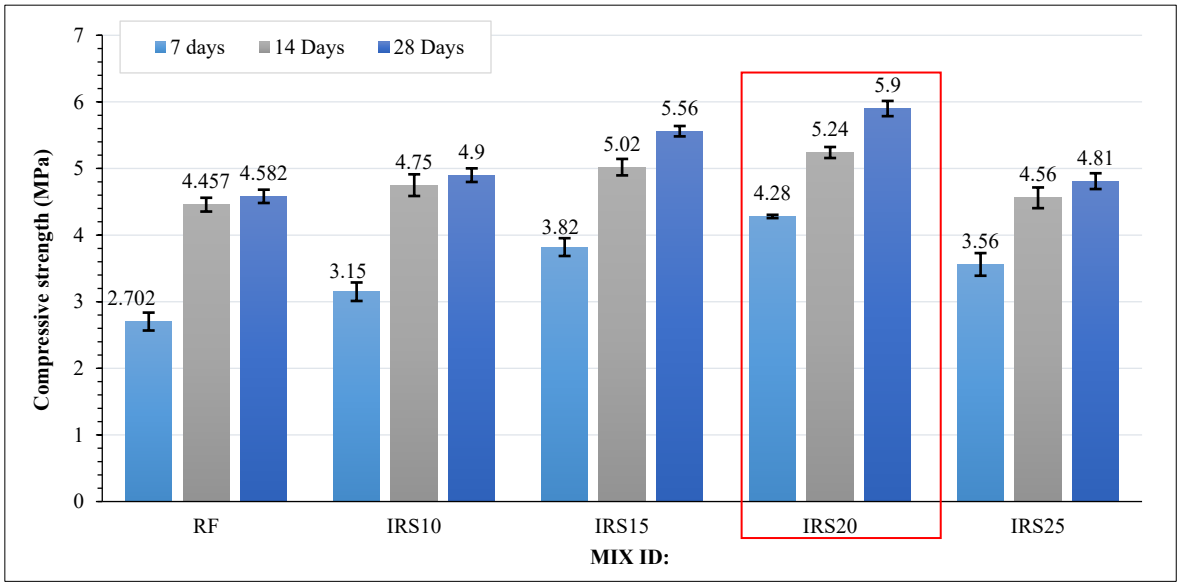

Figure 14. Compressive Strength of Non-Autoclaved Aerated Concrete (NAAC)

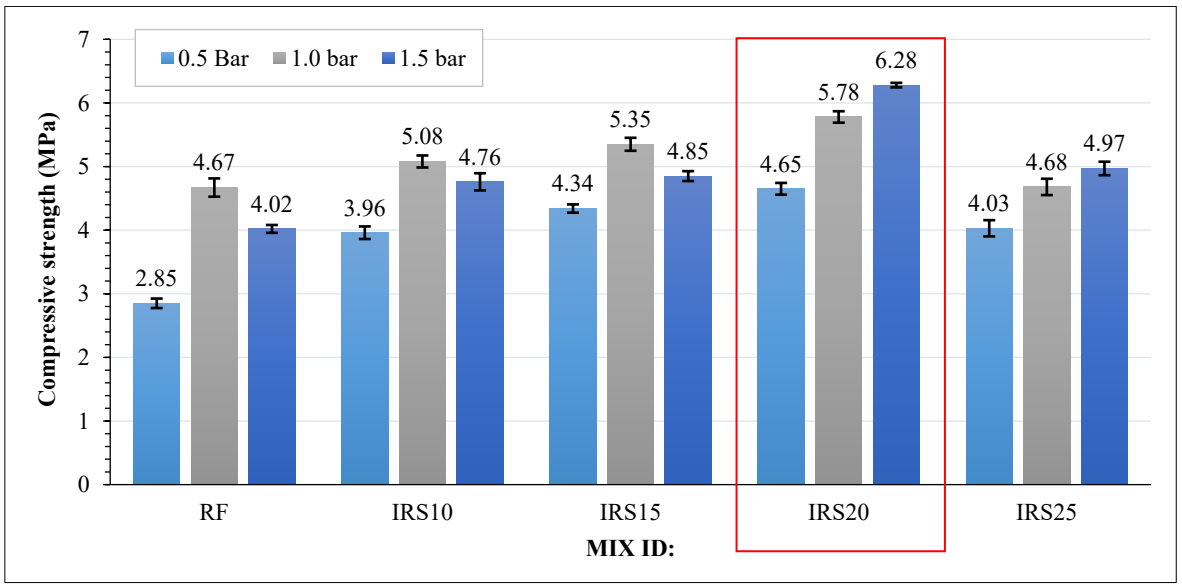

Figure 15. Compressive Strength of Autoclaved Aerated Concrete (AAC)

3.3. Water Absorption of Aerated Concrete

Water absorption serves as an essential indicator for assessing the durability and permeability of concrete, inherently associated with its porosity and microstructural integrity. This study evaluated the water absorption of both AAC and NAAC samples after 28 days of curing, with varied percentages of Indus River Sand (IRS) replacement ranging from 0% to 25%, as illustrated in the Figure 16. The findings demonstrated a constant increase in water absorption correlating with higher IRS content in both AAC and NAAC. For NAAC, absorption rose from 15.2% at 0% IRS to 19.1% at 25% IRS. In AAC, water absorption increased from 13.8% to 17.2% within the same IRS range. This trend can be attributed

to the physical characteristics of IRS, which possesses finer and smoother particles in contrast to the coarser, more angular hill sand. As IRS content increased, the mixture became more permeable due to reduced inter-particle friction and compromised aggregate-paste bonding. This promoted the formation of more capillary gaps, leading to increased water infiltration during immersion testing.

Despite this increasing trend, AAC consistently demonstrated somewhat lower water absorption values than NAAC. The autoclaving technique primarily contributes to this by reducing micro-voids through high-pressure steam curing and facilitating the production of tobermorite. This dense crystalline phase occupies capillary pores and improves impermeability. NAAC, without the autoclaving process, exhibited increased porosity and a weaker microstructure, rendering it more vulnerable to moisture infiltration. These results indicate that while AAC exhibits enhanced resistance to water absorption, NAAC strikes a balance between sufficient durability and increased sustainability. Particularly at IRS replacement levels of 10–15%, NAAC has satisfactory absorption properties while being more energy-efficient and economically advantageous.

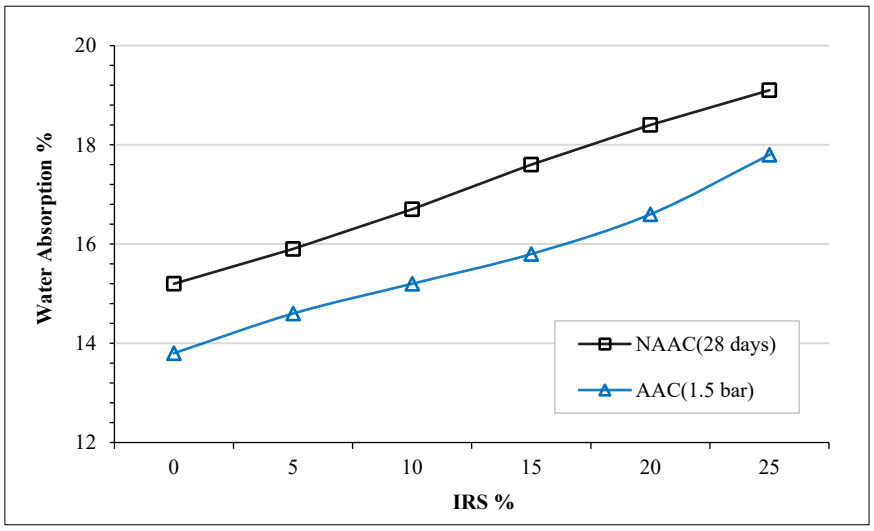

Figure 16. Water Absorption of Aerated Concrete

3.4. Crack Patterns of Aerated Concrete

The crack patterns of the aerated concrete (AAC+NAAC) samples, illustrated in Figure 17, demonstrated a distinct relationship with the proportion of Indus River Sand (IRS) incorporated in the mixture. Sample A, without IRS and entirely composed of hill sand, demonstrated the minimal degree of cracking. Only tiny superficial fissures were apparent, indicating stability, internal cohesion, uniform pore structure, and efficient bonding between the binder and the hill sand particles. Likewise, Sample B, containing 5% IRS, exhibited negligible cracking, with the fracture patterns remaining consistent and controlled. The little IRS content did not substantially compromise the matrix's integrity, and the sample maintained its structural resilience against crack initiation and propagation.

Figure 17. Crack patterns of Aerated Concrete

Nevertheless, as the IRS content increased, significant alterations in crack behaviour began to emerge. Sample C (10% IRS) displayed more pronounced and visible fissures, signifying a deterioration in material integrity. The increased presence of IRS, characterized by a smoother texture and finer grading relative to hill sand, may have reduced frictional resistance and resulted in a compromised microstructure, hence undermining matrix strength. In Sample D (15% IRS), numerous cracks emerged on the surface, creating a network-like pattern indicative of brittle fracture characteristics. The matrix seemed increasingly fractured, indicating a deterioration of the interfacial transition zones and reduced cohesiveness among the components. The extent of the cracking was most pronounced in Samples E and F, which contained 20% and 25% IRS, respectively.

3.5. Failure Patterns of Aerated Concrete

The failure patterns observed in the aerated concrete samples as shown in Figure 18 exhibit a progression in crack orientation and shape that reflects the underlying mechanical behavior and failure mode. In samples with low or no IRS content (e.g., A and B), cracks developed primarily vertically or nearly parallel to the loading axis, which is characteristic of a compressive or flexural failure mode. These vertical or slightly curved cracks indicate that the material maintained structural integrity until reaching its load limit, after which failure occurred due to axial stress concentration. Such patterns suggest ductile behavior, with the matrix absorbing stress without abrupt disintegration.

Figure 18. Failure Patterns of Aerated Concrete

As the IRS content increased (Samples C and D), the crack patterns began to diverge at angles ranging from 30° to 45°, forming diagonal fracture lines that are typical of shear failure. This angle indicates that the material began to fail due to internal sliding along weak planes; a behavior commonly associated with brittle failure and poor cohesion within the microstructure. The appearance of X-shaped or diagonal cracks shows that the material could no longer sustain vertical stress without transverse movement, a direct result of reduced internal bonding caused by excessive fines and poor interlocking from IRS.

In the samples with high IRS content (Samples E and F), the cracks became more branched, irregular, and multi-angled, showing signs of combined tensile-shear failure. The fragmentation and separation of the sample pieces into multiple jagged zones reflect explosive brittle failure, where the concrete matrix has lost its ability to distribute and resist internal stresses. These irregular fracture planes and lack of dominant crack direction suggest a highly porous, weakly bonded material where failure is sudden and uncontrolled. This supports the conclusion that higher IRS content disrupts paste continuity and impairs the formation of strong interfacial transition zones (ITZs), leading to premature, brittle fracture behavior.

3.6. Comparative Analysis of AAC and NAAC

3.6.1. Compressive Strength

It can be observed from Figures 14 and 15, that the trend line of compressive strength is similar in both the cases of NAAC and AAC in terms of optimum hill sand replacement with IRS. Comparing the results, AAC has higher compressive strength than NAAC, but not with a more significant difference. At 20% sand replacement with IRS, AAC has strengths of 4.6, 5.8, and 6.3 MPa at 0.5 Bar, 1.0 Bar, and 1.5 Bar autoclaving pressures, respectively. Comparing the results, compressive strength of AAC at maximum autoclaving pressure (1.5bar) with NAAC at 28 days of

conventional curing, AAC has 10.3% higher strength. It can also be observed that by increasing the autoclaving pressure from 0.5 to1.5bar, compressive strength increases because under the high temperature and pressure, the chemistry of hydration is changed. C–S–H is formed but it is converted to tobermorite ($C_5S_6H_5$) on continued heating, thus increased strength can be obtained. This is aligned with the approach adopted by Yazal et al. [54]. This change is because high-pressure steam curing causes better hydration of binder and creates better CSH gel in the concrete matrix, which improves the compressive strength of concrete, consistent with previous studies [55, 56].

The compressive strength of the mixes showed a general increase up to a certain point of IRS replacement, followed by a decline. For both AAC and NAAC, the optimal performance was observed around 15–20% IRS replacement. This increase in strength can be attributed to the filler effect of fine IRS particles, which initially reduced internal voids, resulting in improved strength.

In AAC, the autoclaving process further contributed to this strength gain by encouraging crystalline bond formation around the finer particles, particularly at the interfacial transition zones (ITZs). However, as IRS content increased beyond 15%, a decline in compressive strength was observed. This is likely due to increased porosity and reduced matrix cohesion, as IRS particles tend to absorb more water and offer less surface roughness for mechanical interlocking. The excess fines may also hinder proper hydration of cementitious materials, weakening the internal structure.

In NAAC, the compressive strength trend followed a similar pattern, but the peak strength values were generally lower. This is due to the absence of autoclaving, which limits the densification and phase transformation of the cement matrix. Without thermal curing, the finer IRS content creates a more fragile pore network, which contributes to early crack propagation under stress.

These findings confirm that IRS can be beneficial as a partial sand replacement up to a limited percentage, after which it begins to negatively affect the structural performance due to microstructural instability.

3.6.2. Environmental Impact Assessment Comparison of AAC and NAAC

Cement manufacturing contributes approximately 7- 10% of global CO_2 emissions. A substantial amount of carbon dioxide is released during the preparation of raw materials for concrete production, despite its widespread use as a construction material. Ordinary Portland cement (OPC), the primary binder in concrete, accounts for 75-82% of the total CO_2 emissions generated by concrete. As a result, researchers have focused on developing alternative materials to reduce these emissions. One promising approach is using waste materials as substitutes for cement and aggregates. While embodied carbon is generated by transporting, processing, and screening these waste materials, their carbon footprint is generally much lower than that of cement and aggregates. By incorporating waste materials with cement-like properties, the total CO_2 emissions from concrete production can be reduced. For example, the study mentioned above utilized FA as a binder substitute. The study also calculates the total CO_2 emissions based on the CO_2 equivalent emissions of each component. Table 4 presents the CO_2 emissions per kilogram for each material, considering the production, transportation, and mixing processes.

Table 4. CO_2 emissions of materials per kilogram

Material	$KgCO_2/Kg$	Reference
OPC	0.82-0.93	Zhu [57]; Turner & Collins [58]
Fly ash	0.027	Turner & Collins [58]
Aluminium	16.6-18.3	Fredriksson [59]
Hill Sand	0.00551-0.0139	Report on National Stone Sand & Gravel Association [60]; Turner & Collins [58]
River Sand	0.0046	Sukontasukkul [61]
Lime	0.75	Bing et al. [62]
Autoclaving Process	0.154	The European Autoclaved Aerated Concrete Association [63]

The total embodied CO_2 values for each concrete mix were calculated by multiplying the amount of each material used to produce 1 m^3 of concrete by the corresponding CO_2 emissions per kilogram of that material. These values were then summed to determine the total embodied CO_2 for the mix. Table 5 illustrates the impact of AAC and NAAC components, including FA and Indus River sand, on embodied CO_2 emissions used in this research. The results show that replacing 50% of cement with FA and 20% River sand reduces the CO_2 emissions to 440.084 $kgCO_2/m^3$, and 393.284 $kgCO_2/m^3$ in AAC and NAAC respectively, causing reduction of 31.91% and 39.22% CO_2 emissions respectively, compared to 20% FA replacement mostly done in literature which caused about 647.499 $kgCO_2/m^3$ CO_2 emissions**.**

Table 5. Total CO_2 emissions emitted to produce $1m^3$ AAC

Material	$KgCO_2/Kg$	Reference	CO_2 emissions per $1m^3$ of concrete ($KgCO_2/m^3$)		
			20FA Conventional method of AAC	50FA20 IRS AAC	50FA20IRS NAAC
OPC	0.93	Zhu [57]; Turner & Collins [58]	513.36	320.85	320.85
Fly ash	0.027	Turner & Collins [58]	3.726	9.315	9.315
Aluminum	18.7	Fredriksson [59]	54.193	25.806	25.806
Hill sand	0.0139 max:	Turner & Collins [58]	13.205	10.564	10.564
River Sand	0.0046	Sukontasukkul [61]	--	0.874	0.874
Lime	0.75	Bing et al. [62]	16.215	25.875	25.875
Autoclaving Process	0.154	The European Autoclaved Aerated Concrete Association [63]	46.8	46.8	--
TOTAL			**647.499**	**440.084**	**393.284**

3.7. Comparison of Present and Previous Studies

The detailed comparison of aerated concrete research shows that while several studies have achieved higher compressive strength, the present study offers one of the most balanced approaches combining strength, durability and sustainability given in Table 6.

Table 6. Comparison of Present Study with Selected Previous Aerated Concrete Investigations

Study	Type	Key Additives/ Replacements	Max Strength (MPa)	Water Absorption (%)	Durability	Sustainability Notes
Present Study	AAC/NAAC	50% FA, 20% IRS	6.28	19.1		Low-cost, reduced CO_2 by 32–39%
Stel'makh et al. [64]	NAAC	16% Microsilica	13.2	-	Good; dense microstructure	High performance, high cost
Ramamurthy & Narayanan [27]	AAC/NAAC	Fly ash, lime	7.8	~20–30	Varies; better in AAC	Established baseline; limited savings
Pachideh & Gholhaki [65]	AAC	Silica fume, GBFS, zeolite	10	≤15	Improved with SF/GBFS	Effective, but uses costly additives
Bukhari et al. [66]	NAAC	30% GGBS, 30% RHA	11	~12	Good durability & thermal insulation	Waste-based, ~30% cheaper than AAC
Narattha et al. [67]	NAAC	30% FA + 10% SF	23	Not reported	Not specifically studied	High strength, but costly ternary system

A comprehensive comparison of previous studies with the present research reveals diverse strategies to enhance the properties of aerated concrete. Stel'makh et al. [64] achieved a maximum compressive strength of 13.2 MPa in NAAC using 16% micro silica as a partial cement replacement. Although this represents a notable improvement in strength, the reliance on micro silica which is a relatively expensive and less commonly available additive, raises concerns about the economic feasibility and scalability of such a mix. Similarly, Narattha et al. [67] reported strengths of NAAC as high as 23 MPa using a ternary blend of 30% fly ash and 10% silica fume. While the performance was outstanding, the cost and sensitivity of such high-performance additives make the system less practical for general-purpose or large-scale application, especially in developing countries.

In contrast, Ramamurthy and Narayanan [27] presented early work on AAC and NAAC, reporting compressive strengths of up to 7.8 MPa for AAC and approximately 3.9 MPa for NAAC using fly ash and variations in sand grading. However, their work also recorded higher water absorption, often exceeding 20%, suggesting a porous matrix and limited durability, particularly in non-autoclaved mixes. Pachideh & Gholhaki [65] explored the use of pozzolanic materials like silica fume, zeolite, and GBFS in AAC, achieving compressive strengths exceeding 10 MPa. Though technically effective, the dependency on multiple high-grade additives adds complexity and cost to the mix design. More recently, Bukhari et al. [66] investigated NAAC blocks made with 30% GGBS and 30% RHA, attaining strengths around 11 MPa and highlighting cost savings of up to 30% compared to AAC and conventional red bricks. Their study reinforces the importance of waste material utilization but does not provide a quantified carbon emission analysis.

In comparison, the present study successfully combines performance and sustainability by using 50% fly ash and 20% Indus River Sand to achieve compressive strengths of 6.28 MPa (AAC) and 5.9 MPa (NAAC), which are competitive within the range of earlier works. Importantly, water absorption remained within acceptable limits (19.1%), indicating satisfactory durability. Moreover, the formulation resulted in a verified CO_2 emission reduction of 32% for AAC and 39.3% for NAAC; a key sustainability metric not quantified in most of the previous literature. While some

studies exceeded these strength values, they often did so at the cost of economic and material practicality. By contrast, the present mix design is not only technically sound but also affordable, locally available, and easily adaptable for real-world construction. This makes it particularly suitable for low-cost, sustainable infrastructure in regions where environmental and economic constraints are significant.

In addition to performance, the production cost of the optimal mix was also considered. The optimized mix proposed in this study demonstrates a clear cost advantage over conventional aerated concrete which is AAC. Material costs were significantly reduced by substituting 50% of OPC with fly ash and 20% of hill sand with Indus River Sand, as FA is free of cost in our region being waste product, and IRS costed only transportation charges. Moreover, in AAC, the use of controlled autoclaving at relatively low pressures (0.5–1.5 bar) reduced energy input compared to traditional high-pressure steam curing typically 180–190 °C at 12–13 bar pressure for 5–6 hours in conventional AAC manufacturing. NAAC further minimizes energy costs through ambient-temperature curing. Therefore, both mixes—especially NAAC—offer notable reductions in material and energy-related production costs compared to conventional AAC. In contrast, the NAAC mix in this study achieved comparable strength (5.9 MPa) while reducing CO_2 emissions by 39.3% and production costs by an estimated 25–35%, confirming its suitability as a more sustainable and economically viable alternative to conventional AAC.

4. Conclusions

This research was conducted to evaluate innovative advancement in the construction industry through the utilization of IRS and find its optimum conditions as a partial substitute for hill sand. This research used different percentages of IRS by weight of hill sand in Aerated concrete. Two kinds of AC were developed, i.e., AAC and NAAC, to find the most suitable. Considering the excess CO_2 emission due to cement production, innovation, and sustainability, fly ash was also incorporated as CRM with a ratio of 50% to the weight of cement. The following conclusions were drawn from this experimental study based on the experimental results.

- The EDS of the FA sample suggests that it is classified as Class F. This conclusion is based on the prominent presence of crystalline phases such as quartz (SiO_2), mullite ($3Al_2O_3•2SiO_2$), and hematite (Fe_2O_3), which are characteristic of Class F FA. Additionally, the low calcium content, inferred from the absence or minimal presence of calcium-bearing minerals like lime (CaO), further supports this.
- The XRD analysis of the FA sample indicates that it is predominantly amorphous, as evidenced by the broad hump in the XRD pattern, typically centered around 15-50 degrees 2θ. Additionally, the presence of mild peaks corresponding to crystalline phases, such as quartz (SiO_2), mullite ($3Al_2O_3•2SiO_2$), and hematite (Fe_2O_3) suggests it contains small amounts of crystalline components. The low intensity and sharpness of these peaks further support the predominance of the amorphous phase in FA.
- FA was used as CRM by 50% as a binder by weight of OPC. Due to FA and IRS being finer than OPC and Hill sand respectively, produced denser aerated concrete, as Binder: Sand ratio was kept constant throughout, which led to reduced aeration and increased density.
- Replacing hill sand with IRS from the Kotri barrage vicinity significantly improved compressive strength in both autoclaved and non-autoclaved aerated concrete. The peak compressive strength of 5.87 MPa (NAAC) and 6.28 MPa (AAC) was achieved at 20% IRS substitution (IRS20), marking a notable 28.76% and 56.21% increase over the reference specimen (0% IRS) for NAAC and AAC, respectively. This occurred because incorporating the IRS increased the level of gradation of specimens. However, substituting IRS beyond 20% decreased aeration, compressive strength, higher density, and specimen cracking because of uniform gradation depicted by the PSD curve, uniform particle shape depicted by SEM, and additional requirement of cement paste to make better bonding. Additionally, River sand from the regions having similar chemical composition can be effectively used to in the production of AC making it sustainable and retrieving the ecosystem of the globe.
- Incorporating IRS in the specimen increased the density because IRS has a higher specific gravity. The strength at 28 days of conventional curing is approximately equal to that at 1.5 bar pressure autoclaving.
- Crack and failure patterns revealed that the structural behavior of aerated concrete deteriorates with increasing Indus River Sand (IRS) content. Samples with lower IRS percentages exhibited minimal, vertical cracks indicating ductile and stable failure, while those with higher IRS replacement showed wider, diagonal, and irregular cracks, signifying a shift toward brittle and shear-dominated failure. These patterns reflect a loss of internal cohesion at higher IRS levels, highlighting the adverse effect of excessive IRS on the mechanical integrity of aerated concrete.
- Replacing 50% cement with FA resulted in the highest decrease in embodied CO_2 along with 20% River sand. The mix 50FA20IRS proved to be the most efficient option. FA not only decreased the environmental effect but also improved the strength of aerated concrete.

5. Declarations

5.1. Author Contributions

Conceptualization, M.L., A.K., and R.L.; methodology, M.L.; formal analysis, M.L. and A.K.; investigation, M.L.; resources, R.L.; data curation, M.L. and A.K.; writing—original draft preparation, M.L. and A.K.; writing—review and editing, M.L. and R.L.; visualization, A.K. and T.H.A.; supervision, A.K.; project administration, T.H.A.; funding acquisition, A.K. All authors have read and agreed to the published version of the manuscript.

5.2. Data Availability Statement

The data presented in this study are available on request from the corresponding author.

5.3. Funding

The authors would like to appreciate the financial support from the Continental Enterprises, Karachi, Pakistan.

5.4. Acknowledgements

The authors would like to acknowledge and appreciate the support from the Department of Civil Engineering, Mehran University of Engineering and Technology, Jamshoro, Pakistan, and Continental Enterprises, Karachi, Pakistan.

5.5. Conflicts of Interest

The authors declare no conflict of interest.

6. References

[1] Fudge, C. (2011). Designing with AAC to achieve sustainable houses. Management, 9(10), 1-11.

[2] Qu, X., & Zhao, X. (2017). Previous and present investigations on the components, microstructure and main properties of autoclaved aerated concrete – A review. Construction and Building Materials, 135, 505-516. doi:10.1016/j.conbuildmat.2016.12.208.

[3] Kreft, O. (2017). Autoclaved aerated concrete with sulphate content: an environmentally friendly, durable and recyclable building material. Mauerwerk, 21(5), 287–296. doi:10.1002/dama.201700012.

[4] Fudge, C., Fouad, F., & Klingner, R. (2019). Autoclaved aerated concrete. Developments in the Formulation and Reinforcement of Concrete, Woodhead Publishing, Sawston, United Kingdom. doi:10.1016/b978-0-08-102616-8.00015-0.

[5] Mindess, S. (2019). Developments in the formulation and reinforcement of concrete. Developments in the Formulation and Reinforcement of Concrete. Woodhead Publishing. doi:10.1016/C2017-0-03347-5.

[6] Hendry, E. A. W. (2001). Masonry walls: materials and construction. Construction and Building Materials, 15(8), 323–330. doi:10.1016/s0950-0618(01)00019-8.

[7] Hess, J. A., Kincl, L., Amasay, T., & Wolfe, P. (2010). Ergonomic evaluation of masons laying concrete masonry units and autoclaved aerated concrete. Applied Ergonomics, 41(3), 477–483. doi:10.1016/j.apergo.2009.10.003.

[8] Phonphuak, N., & Chindaprasirt, P. (2015). Types of waste, properties, and durability of pore-forming waste-based fired masonry bricks. Eco-Efficient Masonry Bricks and Blocks, 103–127, Woodhead Publishing, Sawston, United Kingdom. doi:10.1016/b978-1-78242-305-8.00006-1.

[9] Radhi, H. (2011). Viability of autoclaved aerated concrete walls for the residential sector in the United Arab Emirates. Energy and Buildings, 43(9), 2086–2092. doi:10.1016/j.enbuild.2011.04.018.

[10] Holt, E., & Raivio, P. (2005). Use of gasification residues in aerated autoclaved concrete. Cement and Concrete Research, 35(4), 796–802. doi:10.1016/j.cemconres.2004.05.005.

[11] DIN EN 771-4:2015-11. (2015). Specification for masonry units - Part 4: Autoclaved aerated concrete masonry units. Deutsches Institut für Normung (DIN), Berlin, Germany. (In German).

[12] BS EN 771-4:2011+A1:2015. (2011). Specification for masonry units - Autoclaved aerated concrete masonry units. British Standards Institution (BSI), London, United Kingdom.

[13] Wongkeo, W., & Chaipanich, A. (2010). Compressive strength, microstructure and thermal analysis of autoclaved and air cured structural lightweight concrete made with coal bottom ash and silica fume. Materials Science and Engineering: A, 527(16–17), 3676–3684. doi:10.1016/j.msea.2010.01.089.

[14] Thongtha, A., Maneewan, S., Punlek, C., & Ungkoon, Y. (2014). Investigation of the compressive strength, time lags and decrement factors of AAC-lightweight concrete containing sugar sediment waste. Energy and Buildings, 84, 516–525. doi:10.1016/j.enbuild.2014.08.026.

[15] Bonakdar, A., Babbitt, F., & Mobasher, B. (2013). Physical and mechanical characterization of Fiber-Reinforced Aerated Concrete (FRAC). Cement and Concrete Composites, 38, 82–91. doi:10.1016/j.cemconcomp.2013.03.006.

[16] Lam, N. N. (2021). Recycling of AAC Waste in the Manufacture of Autoclaved Aerated Concrete in Vietnam. International Journal of GEOMATE, 20(78), 128–134. doi:10.21660/2021.78.j2048.

[17] Demirboğa, R. (2007). Thermal conductivity and compressive strength of concrete incorporation with mineral admixtures. Building and Environment, 42(7), 2467–2471. doi:10.1016/j.buildenv.2006.06.010.

[18] Demirboğa, R., & Gül, R. (2003). The effects of expanded perlite aggregate, silica fume and fly ash on the thermal conductivity of lightweight concrete. Cement and Concrete Research, 33(5), 723–727. doi:10.1016/S0008-8846(02)01032-3.

[19] Demirboğa, R. (2003). Influence of mineral admixtures on thermal conductivity and compressive strength of mortar. Energy and Buildings, 35(2), 189–192. doi:10.1016/S0378-7788(02)00052-X.

[20] Shrivastava O. P. (1977). Lightweight aerated concrete – a review. Indian Concrete Journal, 51, 10–23.

[21] Xia, Y., Yan, Y., & Hu, Z. (2013). Utilization of circulating fluidized bed fly ash in preparing non-autoclaved aerated concrete production. Construction and Building Materials, 47, 1461–1467. doi:10.1016/j.conbuildmat.2013.06.033.

[22] Narayanan, N., & Ramamurthy, K. (2000). Structure and properties of aerated concrete: A review. Cement and Concrete Composites, 22(5), 321–329. doi:10.1016/S0958-9465(00)00016-0.

[23] Narayanan, N., & Ramamurthy, K. (2000). Microstructural investigations on aerated concrete. Cement and Concrete Research, 30(3), 457–464. doi:10.1016/S0008-8846(00)00199-X.

[24] Valore, R. C. (1954). Cellular Concretes Part 1 Composition and Methods of Preparation. ACI Journal Proceedings, 50(5), 773–796. doi:10.14359/11794.

[25] Aroni, S., Groot, G. J., Robinson, M. J., Svanholm, G., & Wittman, F. H. (1993). RILEM Recommended Practice: Autoclaved Aerated Concrete, Properties, Testing and Design. Chapman & Hall, London, United kingdom.

[26] Lashari, A. R., Kumar, A., Kumar, R., & Rizvi, S. H. (2023). Combined effect of silica fume and fly ash as cementitious material on strength characteristics, embodied carbon, and cost of autoclave aerated concrete. Environmental Science and Pollution Research, 30(10), 27875–27883. doi:10.1007/s11356-022-24217-9.

[27] Ramamurthy, K., & Narayanan, N. (2000). Factors influencing the density and compressive strength of aerated concrete. Magazine of Concrete Research, 52(3), 163–168. doi:10.1680/macr.2000.52.3.163.

[28] Blanco, F., Garciéa, P., Mateos, P., & Ayala, J. (2000). Characteristics and properties of lightweight concrete manufactured with cenospheres. Cement and Concrete Research, 30(11), 1715–1722. doi:10.1016/S0008-8846(00)00357-4.

[29] Xie, Y., Zhou, H., Wang, J., Meng, H., Wei, S., Sun, J., & Hu, Y. (2025). Enhancing autoclaved aerated concrete performance via replacement of fly ash with granite stone powder and steel slag: Critical role of Ca/Si ratio. Construction and Building Materials, 477, 141360. doi:10.1016/j.conbuildmat.2025.141360.

[30] Jerman, M., Keppert, M., Výborný, J., & Černý, R. (2013). Hygric, thermal and durability properties of autoclaved aerated concrete. Construction and Building Materials, 41, 352–359. doi:10.1016/j.conbuildmat.2012.12.036.

[31] Tikalsky, P. J., Pospisil, J., & MacDonald, W. (2004). A method for assessment of the freeze-thaw resistance of preformed foam cellular concrete. Cement and Concrete Research, 34(5), 889–893. doi:10.1016/j.cemconres.2003.11.005.

[32] Abdullah, K., Hussin, M. W., Zakaria, F., Muhamad, R., & Abdul Hamid, Z. (2006). POFA: A potential partial cement replacement material in aerated concrete. Proceedings of the 6th Asia-Pacific Structural Engineering and Construction Conference, 5-6 September, 2006, Kuala Lumpur, Malaysia.

[33] Rahman, R. A., Fazlizan, A., Asim, N., & Thongtha, A. (2021). A review on the utilization of waste material for autoclaved aerated concrete production†. Journal of Renewable Materials, 9(1), 61–72. doi:10.32604/jrm.2021.013296.

[34] Kurama, H., Topçu, I. B., & Karakurt, C. (2009). Properties of the autoclaved aerated concrete produced from coal bottom ash. Journal of Materials Processing Technology, 209(2), 767–773. doi:10.1016/j.jmatprotec.2008.02.044.

[35] Dey, P., Paul, A., Dhar, M., Das, D., & Saha, R. (2025). State-of-art review and future prospects of autoclave aerated concrete for building a sustainable tomorrow. Environment, Development and Sustainability, 1–42,. doi:10.1007/s10668-025-06194-4.

[36] Wei, C., Wu, P., Gu, J., Liu, X., Zhang, Z., Li, S., & Shao, Y. (2025). Potential of titanium gypsum in autoclaved aerated concrete for large incorporation: Hydration characteristics and performance optimization. Construction and Building Materials, 473, 140995. doi:10.1016/j.conbuildmat.2025.140995.

[37] Sun, R., Shen, P., Zhang, X., Qin, Q., Tao, Y., Wang, D., Liu, Z., & Poon, C. sun. (2025). Effects of curing regimes and binder designs on steel slag-based carbonated aerated concrete (CAC): Reaching a balance between pre-hydration and carbonation. Cement and Concrete Research, 195, 107905. doi:10.1016/j.cemconres.2025.107905.

[38] Chen, C., Liu, X., Wang, X., Jiu, S., Chen, Y., & Liu, Y. (2025). Development of sustainable non-autoclaved aerated concrete: Influence of aluminium powder on mechanical properties and pore structure of geopolymers based on rockwool furnace bottom slag waste. Construction and Building Materials, 472, 140957. doi:10.1016/j.conbuildmat.2025.140957.

[39] Peng, F., Chen, C., Jiu, S., Song, Q., & Chen, Y. (2024). Preparation and Characterization of Novel Sulfoaluminate-Cement-Based Nonautoclaved Aerated Concrete. Materials, 17(4), 836. doi:10.3390/ma17040836.

[40] Shon, C. S., Mukangali, I., Zhang, D., Ulykbanov, A., & Kim, J. (2021). Evaluation of non-autoclaved aerated concrete for energy behaviors of a residential house in Nur-Sultan, Kazakhstan. Buildings, 11(12), 610. doi:10.3390/buildings11120610.

[41] Bhatawdekar, R. M., Singh, T. N., Tonnizam Mohamad, E., Armaghani, D. J., & Binti Abang Hasbollah, D. Z. (2021). River Sand Mining Vis a Vis Manufactured Sand for Sustainability. Proceedings of the International Conference on Innovations for Sustainable and Responsible Mining, Lecture Notes in Civil Engineering, 109, Springer, Cham, Switzerland. doi:10.1007/978-3-030-60839-2_8.

[42] Sangoju, B., Ramesh, G., Bharatkumar, B. H., & Ramanjaneyulu, K. (2017). Evaluation of Durability Parameters of Concrete with Manufacture Sand and River Sand. Journal of The Institution of Engineers (India): Series A, 98(3), 267–275. doi:10.1007/s40030-017-0204-4.

[43] Lakhiar, M. T., Mohamad, N., Shaikh, M. A. B., Vighio, A. A., Jhatial, A. A., & Abdul Samad, A. A. (2018). Effect of River Indus Sand on Concrete Tensile Strength. Engineering, Technology & Applied Science Research, 8(2), 2796–2798. doi:10.48084/etasr.1869.

[44] Kunchariyakun, K., Asavapisit, S., & Sinyoung, S. (2018). Influence of partial sand replacement by black rice husk ash and bagasse ash on properties of autoclaved aerated concrete under different temperatures and times. Construction and Building Materials, 173, 220–227. doi:10.1016/j.conbuildmat.2018.04.043.

[45] Serhat Baspinar, M., Demir, I., Kahraman, E., & Gorhan, G. (2014). Utilization potential of fly ash together with silica fume in autoclaved aerated concrete production. KSCE Journal of Civil Engineering, 18(1), 47–52. doi:10.1007/s12205-014-0392-7.

[46] Baturin, G. N., & Gordeev, V. V. (2019). Geochemistry of Suspended Matter in the Amazon River Waters. Geochemistry International, 57(2), 197–205. doi:10.1134/S0016702919020022.

[47] Ali, M. H., Aal, A. A. El, Radwan, A. E., & Saber, E. S. A. (2024). Geochemistry and mineralogy of modern floodplain Nile sediments of Sohag area, Egypt: an environmental perspective. Environmental Earth Sciences, 83(11), 350. doi:10.1007/s12665-024-11638-7.

[48] Channa, M. Y., Anwar, J., Kalsoom, R., & Abidi, S. H. I. (2024). Qualitative analysis of rivers sand sources (Silica sand, Ravi river sand, Indus river sand, and Jhelum river sand) for metal casting: a comparative study. Engineering Research Express, 6(3), 35435. doi:10.1088/2631-8695/ad7cc2.

[49] Verma, A. (2015). Evaluation of sea sand and river sand properties and their comparison. National Dong Hwa University, 1-36. doi:10.13140/RG.2.1.4906.6327.

[50] ASTM C150/C150M-12. (2015). Standard Specification for Portland Cement. ASTM International, Pennsylvania, United States. doi:10.1520/C0150_C0150M-12.

[51] Raj, I. S., & John, E. (2019). Evaluation of properties of aerated concrete partially replaced by cement with fly ash. International Journal of Advanced Research in Engineering and Technology, 10(1), 223–229. doi:10.34218/IJARET.10.1.2019.022.

[52] Li, G., Zhou, C., Ahmad, W., Usanova, K. I., Karelina, M., Mohamed, A. M., & Khallaf, R. (2022). Fly Ash Application as Supplementary Cementitious Material: A Review. Materials, 15(7), 2664. doi:10.3390/ma15072664.

[53] ASTM C618-17a. (2019). Standard Specification for Coal Fly Ash and Raw or Calcined Natural Pozzolan for Use in Concrete. ASTM International, Pennsylvania, United States. doi:10.1520/C0618-17A.

[54] Yazal, A., Kavas, T., & Soyal, A. D. (2018). Effects of different autoclaving pressure on mechanical properties of AAC. Ce/Papers, 2(4), 591–594. doi:10.1002/cepa.829.

[55] Zdeb, T. (2017). An analysis of the steam curing and autoclaving process parameters for reactive powder concretes. Construction and Building Materials, 131, 758–766. doi:10.1016/j.conbuildmat.2016.11.026.

[56] Moslehi, A., Dashti Rahmatabadi, M. A., & Arman, H. (2023). Determination of Optimized Mix Design of Reactive Powder Concrete. Advances in Civil Engineering, 2023, 754–767,. doi:10.1155/2023/4421095.

[57] Zhu, Q. (2011). CO_2 abatement in the cement industry. IEA Clean Coal Centre, London, United Kingdom.

[58] Turner, L. K., & Collins, F. G. (2013). Carbon dioxide equivalent (CO2-e) emissions: A comparison between geopolymer and OPC cement concrete. Construction and Building Materials, 43, 125–130. doi:10.1016/j.conbuildmat.2013.01.023.

[59] Fredriksson, C. (2019). Sustainability of metal powder additive manufacturing. Procedia Manufacturing, 33, 139–144. doi:10.1016/j.promfg.2019.04.018.

[60] National Stone Sand & Gravel Association. (2021). The Aggregates Industry Greenhouse Gases: Low Emissions, High Resiliency. National Stone Sand & Gravel Association, Alexandria, United States.

[61] Sukontasukkul, P. (2009). Methodology for calculating carbon dioxide emission in the production of ready-mixed concrete. The Proceedings of the First International Conference on Computational Technologies in Concrete Structures (CTCS 09), 24-27 May 2009, Jeju, Korea.

[62] Bing, L., Ma, M., Liu, L., Wang, J., Niu, L., & Xi, F. (2023). An investigation of the global uptake of CO2 by lime from 1930 to 2020. Earth System Science Data, 15(6), 2431–2444,. doi:10.5194/essd-15-2431-2023.

[63] Turski, R. (2022). EAACA net-zero roadmap for autoclaved aerated concrete. Ce/Papers, 5(5), 48-52. doi:10.1002/cepa.1876.

[64] Stel'makh, S. A., Shcherban', E. M., Beskopylny, A. N., Mailyan, L. R., Meskhi, B., Beskopylny, N., Dotsenko, N., & Kotenko, M. (2022). Influence of Recipe Factors on the Structure and Properties of Non-Autoclaved Aerated Concrete of Increased Strength. Applied Sciences (Switzerland), 12(14), 6984. doi:10.3390/app12146984.

[65] Pachideh, G., & Gholhaki, M. (2019). Effect of pozzolanic materials on mechanical properties and water absorption of autoclaved aerated concrete. Journal of Building Engineering, 26(February), 100856. doi:10.1016/j.jobe.2019.100856.

[66] Bukhari, S. A., Patil, D., Gogate, N. G., & Minde, P. R. (2023). Utilization of waste materials in non-autoclaved aerated concrete blocks: State of art review. Materials Today: Proceedings. doi:10.1016/j.matpr.2023.02.334.

[67] Narattha, C., Thongsanitgarn, P., & Chaipanich, A. (2015). Thermogravimetry analysis, compressive strength and thermal conductivity tests of non-autoclaved aerated Portland cement-fly ash-silica fume concrete. Journal of Thermal Analysis and Calorimetry, 122(1), 11–20. doi:10.1007/s10973-015-4724-8.